Tech Science Press

# Chaotic Krill Herd with Deep Transfer Learning-Based Biometric Iris Recognition System

**Harbi Al-Mahafzah[1], Tamer AbuKhalil[1] and Bassam A. Y. Alqaralleh[2,*]**

[1]Department of Computer Science, Faculty of Information Technology, Al-Hussein Bin Talal University Ma'an, 71111, Jordan
[2]MIS Department, College of Business Administration, University of Business and Technology, Jeddah, 21448, Saudi Arabia
*Corresponding Author: Bassam A. Y. Alqaralleh. Email: b.alqaralleh@ubt.edu.sa

**Abstract:** Biometric verification has become essential to authenticate the individuals in public and private places. Among several biometrics, iris has peculiar features and its working mechanism is complex in nature. The recent developments in Machine Learning and Deep Learning approaches enable the development of effective iris recognition models. With this motivation, the current study introduces a novel Chaotic Krill Herd with Deep Transfer Learning Based Biometric Iris Recognition System (CKHDTL-BIRS). The presented CKHDTL-BIRS model intends to recognize and classify iris images as a part of biometric verification. To achieve this, CKHDTL-BIRS model initially performs Median Filtering (MF)-based preprocessing and segmentation for iris localization. In addition, MobileNet model is also utilized to generate a set of useful feature vectors. Moreover, Stacked Sparse Autoencoder (SSAE) approach is applied for classification. At last, CKH algorithm is exploited for optimization of the parameters involved in SSAE technique. The proposed CKHDTL-BIRS model was experimentally validated using benchmark dataset and the outcomes were examined under several aspects. The comparison study results established the enhanced performance of CKHDTL-BIRS technique over recent approaches.

**Keywords:** Biometric verification; iris recognition; deep learning; parameter tuning; machine learning

## 1 Introduction

Security sciences have started leveraging interesting elements for the past few years to ensure secure admission to confined places since it has become a crucial issue. The rising interest upon effective security confirmation frameworks has boosted the development of verification frameworks that are safer and highly proficient [1,2]. Conventional ways to deal with Iris Detection (ID), for example, utilization of a key or secret phrase is unacceptable in selected applications. This is due to the fact that these techniques can undoubtedly be neglected, taken, or broken. To conquer these shortcomings, the

mechanization of distinguishing proof frameworks is applied with the help of biometric methods [3]. The requirement for dependable and secure frameworks has prompted the rise of physiological and social models in biometric frameworks. Iris Recognition System (IRS) framework is highly effective in nature and it is a solid framework to check the reality [4]. It can be enclosed by means of a design in such a way that it can influence an individual's wellbeing. Further, it can be implemented through a painless gadget [5]. As a result, some futuristic organizations that deal with security have already started anticipating the fate of IRS, because of its wide applications and capability of innovation.

The primary reason behind considering iris for biometric verification is that it is one of the truly-steady biometric feature that barely changes in the lifetime of human being [6]. Subsequently, iris locale can be successfully constructed and used for recognition or ID [7]. There is enormous scope available for projects that distinguish public and the need for appropriate biometric recognition is progressively conveyed across the globe. Public ID programs are progressively using IRS for better accuracy and dependability to enroll the residents (notwithstanding, the usage of various biometric recognition methods like two-layered face and unique mark recognition framework). IRS is a high-precision confirmation approach whilst its high potentials are yet to be unleashed [8].

IRS is being progressively applied in robotized frameworks especially in security. In this regard, most of the nations started utilizing IRS to enhance security at entry checkpoints such as air terminals and boundaries, at government entities like medical clinics and even in cell phones too [9]. Albeit, a significant number of past works conducted upon IRS accomplish high precision rates. It includes huge pre-processing tasks (counting iris division and unwrapping the first iris into a rectangular region) and utilization of a few hands-tailored highlights. However, this may not be ideal for different iris datasets, collected under different lighting and ecological circumstances. Lately, there has been a great deal of spotlight on creating models to learn the elements together. In line with this, Deep Learning (DL) models have been exceptionally effective in different computer vision tasks [10].

Zhao et al. [11] presented a DL approach based on capsule network structure in IRS. In this infrastructure, the network features are adjusted after which a different routing technique is offered based on dynamic routing between two capsule layers. This is done so to make this approach, a suitable one for IRS. Adamović et al. [12] proposed a novel IRS model based on Machine Learning (ML) approaches. The motivation behind this research belongs to the association between biometric schemes and stylometry as demonstrated in literature. The purposes of the presented technique are to achieve high classification accuracy, remove false acceptance rate, and cancel the probability of recreating iris image in a created template. Ahmadi et al. [13] presented an extravagant IRS approach based on a group of two-dimension Gabor kernel (2-DGK), Step Filtering (SF), and Polynomial Filtering (PF) to extract the features and hybrid Radial Basis Function Neural Network (RBFNN) with Genetic Algorithm (GA) to perform equivalent tasks. In literature [14], the authors examined a novel DL-based model for IRS and attempted to improve the accuracy with the help of basic infrastructure in order to recover the representative feature. It can be assumed that the residual network learns with dilated convolution kernel during the optimization of training method and aggregation of contextual data in iris image. In the study conducted earlier [15], the authors proposed a structure to capture real-time IRS and perform segmentation from video as part of biometric detection model. The method concentrates on image capture, IRS, and segmentation from video frame in a controlled manner. The criteria include border and access control while the people collaborate from different detection procedures.

The current study introduces a novel Chaotic Krill Herd with Deep Transfer Learning Based Biometric Iris Recognition System (CKHDTL-BIRS). The aim of the presented CKHDTL-BIRS

model is to recognize and classify iris images for biometric verification. To achieve this, CKHDTL-BIRS model initially performs Median Filtering (MF)-based preprocessing and segmentation for iris localization. In addition, MobileNet model is utilized to generate a set of useful feature vectors. Moreover, Stacked Sparse Autoencoder (SSAE) technique is also applied for classification. At last, CKH algorithm is exploited for the optimization of parameters involved in SSAE technique. The proposed CKHDTL-BIRS model was experimentally validated using benchmark dataset and the outcomes were inspected under several aspects.

Rest of the paper is organized as follows. Section 2 discusses about the proposed model and Section 3 offers the experimental validation. Finally, Section 4 concludes the work.

## 2 The Proposed Model

In this study, a novel CKHDTL-BIRS technique has been developed to recognize and classify iris for biometric verification. Initially, Median Filter-based preprocessing of the data is performed in CKHDTL-BIRS model after which segmentation is performed to localize iris regions. Besides, MobileNet model is utilized to generate a suitable group of feature vectors. Moreover, CKH with SSAE technique is also executed for classification. Fig. 1 illustrates the block diagram of CKHDTL-BIRS technique.
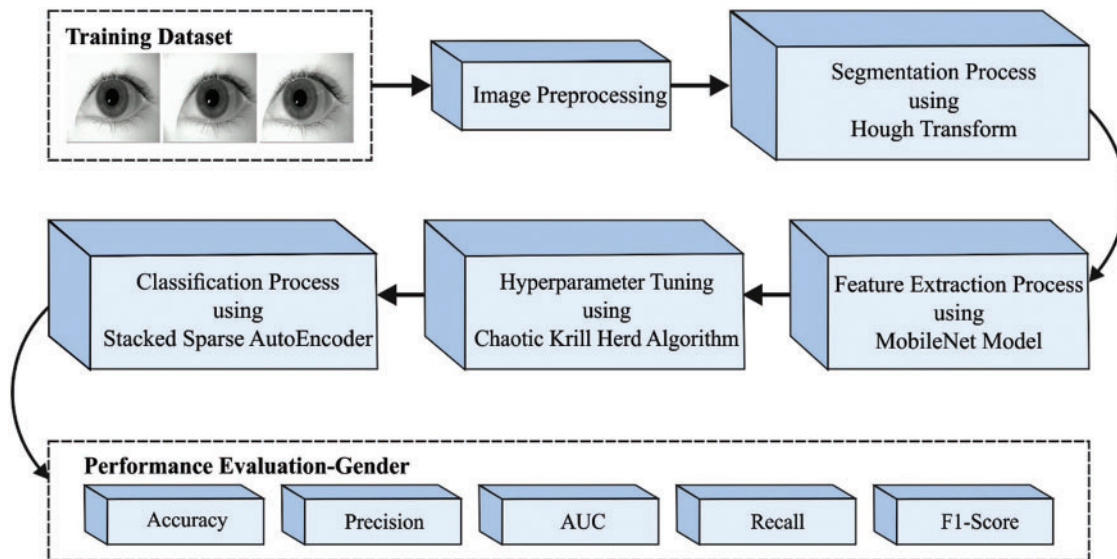


**Figure 1:** Block diagram of CKHDTL-BIRS technique

### 2.1 Image Preprocessing

At the initial stage, the input image is preprocessed through MF technique to remove the noise. MF approach is determined as a nonlinear signal processing method that depends on existing statistics. The MF outcome is determined to be $g(x, y) = med \{f(x - i, y - j), i, j \in W\}$, whereas $f(x, y)$, $g(x, y)$ refers to actual and the last images correspondingly, $W$ demonstrates 2-D mask: with the size of $n \times n$

so as $3 \times 3, 5 \times 5$, etc. MF has non-linear filters while numerical analysis is extremely complex to perform in image with arbitrary noise.

$$\sigma_{med}^2 = \frac{1}{4nf^2\overline{(n)}} \approx \frac{\sigma_i^2}{n + \frac{\pi}{2} - 1} \cdot \frac{\pi}{2} \tag{1}$$

whereas $\sigma_i^2$ refers to input noise power, $n$ signifies the size of MF and $f\overline{(n)}$ denotes the efficiency of noise intensity. Then, the noise variance of average filters is represented as follows.

$$\sigma_0^2 = \frac{1}{n}\sigma_i^2 \tag{2}$$

When (1) and (2) are compared, the results demonstrate that the MF function depends upon two objectives such as size of the mask and noise distribution. MF executes noise removal that is significant, if related to average filters. The function of MF is to maximize, once the MF technique is combined with average filter method.

### 2.2 Iris Segmentation

After preprocessing, segmentation is performed to localize iris regions. The outer radius of iris pattern and pupils are localized primarily with Hough Transform (HT) which contains Canny edge detector to generate edge mapping. HT identifies the place of circles and ellipses; it places contour from 'n' dimension space by investigating whether it can lie on curve of a detailed shape. An identical approach, using parameterized parabolic arcs, is executed to detect upper as well as lower eyelids. Afterwards, the localized iris segment is altered to fixed-size rectangular images.

### 2.3 Feature Extraction

At this stage, MobileNet model is utilized to generate a set of useful feature vectors. MobileNet approach is usually employed in image classification process since it requires minimal computation complexity, compared to other DL methods [16]. The feature vector map is of size $F_m \times F_m$ and the filter is of size $F_s \times F_s$, while the input parameter signifies to $p$, and the resultant parameter is referred to as, $q$. In event of core abstract layer, the entire computational efforts are determined with the help of a parameter $c_e$ and is validated utilizing Eq. (3):

$$c_e = F_s \cdot F_s \cdot \omega \cdot \alpha F_m \cdot \alpha F_m + \omega \cdot \rho \cdot \alpha F_m \cdot \alpha F_m \tag{3}$$

The multiplier value is context-oriented and it lies in the interval of 1 to $n$. The computation effort is defined using the parameter, $cost_e$ and is estimated using Eq. (4):

$$cost_e = F_s \cdot F_s \cdot \omega \cdot \rho \cdot F_m \cdot F_m \tag{4}$$

It integrates depth-wise and point-wise restricted convolutions using depletion parameter which is defined using the parameter $d$, as formulated herewith.

$$d = \frac{F_s \cdot F_s \cdot \omega \cdot \alpha F_m \cdot \alpha F_m + \omega \cdot \cdot \rho \cdot \alpha F_m \cdot \alpha F_m}{F_s \cdot F_s \cdot \omega \cdot \rho \cdot F_m F_m} \tag{5}$$

The size of input image is set to be $224 \times 224 \times 3$. The primary value 2 represents the height and width of the image. The last value refers to the occurrence of three input channels. The projected method takes 32 filters and the size of all filters is established to be $3 \times 3 \times 3 \times 32$.

### 2.4 SSAE Based Iris Recognition

Once the feature vectors are derived, SSAE model is applied for classification. In image classification, the feature vector is provided to SSAE approach so as to allot appropriate class labels. In comparison with Stacked Autoencoder (SAE), SSAE can be trained with the identification of an optimal parameter $\theta = (W, \ b_h, \ b_x)$ in parallel with minimalized discrepancies between reconstruction and input. Once the optimal parameter i.e., $\theta$ is reached, SSAE takes a function: $R^{d_x} \rightarrow R^{d_{h(2)}}$ that transforms the input pixel intensity of image patches to novel feature demonstration $h^{(2)} = f(x) \in R^{d_{h(2)}}$ of nuclear infrastructure. Fig. 2 depicts the framework of SSAE technique.
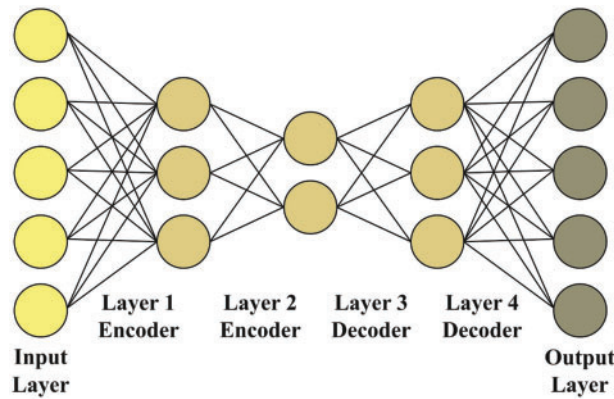


**Figure 2:** Structure of SSAE

In SSAE technique, all the trained patches $x(k)$ of pixel intensity are signified as high level infrastructure portrayal of patches $h^{(2)}(k)$ from the 2$^{nd}$ hidden layer of process. All the trained patches are provided as $\{h^{(2)}(k), \ y(k)\}_{k=1}^{N}$ in which, $k \in \{1, 2, \ldots, N\}$, $\{h^{(2)}(k), \ y(k)\}$ signifies the pair of high level feature and their labels. Two classifier problems are deliberated under this case, while the label of $k^{th}$ patch signifies $y(k) \in \{0, 1\}$, but 0 and 1 define non-nuclear and nuclear patches correspondingly. When considering SSAE learning system, the label data $Y$ is not utilized i.e., SSAE learning is an unsupervised learning model. Once the high level feature learning system is ended, the learned high level depiction and its labels $\{h^{(2)}(k), \ y(k)\}_{k=1}^{N}$ are provided as resultant layer, viz., softmax classification. It can be a supervised approach in which the generalization of Logistic Regression (LR) is as follows [17]:

$$f_{W^{(3)}}(z) = \frac{1}{1 + \exp(-W(3)^{T}z)} \tag{6}$$

Here, $f_{W^{(3)}}(.)$ signifies the sigmoid function using the parameter, $W^{(3)}$. Once the input $z$ of SMC signifies high level depiction of nuclear infrastructure using SSAE, the parameter $W^{(3)}$ is trained using training set $\{h^{(2)}(k), \ y(k)\}_{k=1}^{N}$ to minimize the objective function. With minimalized objective function, assuming $W^{(3)}$ with gradient descent dependent methodology, parameter $W^{(3)}$ is determined.

### 2.5 CKHA Based Parameter Optimization

In this final stage, CKH algorithm is exploited for optimization of the parameters [18,19] involved in SSAE model. Based on swarm behaviour of krill, Krill Herd (KH) algorithm [20], a metaheuristic optimization approach is utilized to resolve optimization problem. In KH, the place is frequently affected by three actions such as,

- Foraging performance;
- Physical diffusion; and
- Effort affected by another krill

In KHA, Lagrangian process is employed from the present searching space as given below.

$$\frac{dX_i}{dr} = N_i + F_i + D_i \tag{7}$$

whereas $N_i$ signifies the motion marked by another individual krill; $F_i$ stands for the foraging motion; and $D_i$ refers to arbitrary diffusion of $i^{th}$ krill individuals.

An initial one, and their direction, $\alpha_i$ are clearly recognized by succeeding parts like repulsive, target, and local effects.

$$N_i^{new} = N^{max}\alpha_i + \omega_n N_i^{old} \tag{8}$$

$N^{max}$, $\omega_n$ and $N_i^{old}$ denote high speed, inertia weight, and final motion correspondingly.

The secondary one is calculated through two elements such as food place and previous experiences. In order to achieve $i^{th}$ krill, it is idealized as follows.

$$F_i = V_f\beta_i + \omega_f F_i^{old} \tag{9}$$

whereas

$$b_i = b_i^{food} + b_i^{best} \tag{10}$$

and $V_f$ signifies the foraging speed, $\omega_f$ denotes inertia weight, and $F_i^{old}$ denotes the last one. The tertiary part is a vital feature among arbitrary processes. It can be estimated based on high diffusion speed and arbitrary directional vectors whereas the equation is provided herewith.

$$D_i = D^{max}\delta \tag{11}$$

Here, $D^{max}$ signifies high diffusion speed, but $\delta$ stands for arbitrary directional vector and its arrays are random numbers. Now, the location in KH from $r$ to $r + \delta r$ is written as follows.

$$X_i(t + Dt) = X_i(t) + Dt\frac{dX_i}{dr} \tag{12}$$

CKHA approach is the resultant product by incorporating chaotic models such as KHA. In this case, a 1D chaotic map is combined with CKHA method.

## 3 Experimental Validation

The proposed CKHDTL-BIRS model was validated for its performance using CASIA iris image database. The results were investigated under five dissimilar runs. Fig. 3 depicts some of the sample images.

Tab. 1 provides the overall recognition performance of MobileNet with SSAE (MN-SSAE) model and CKHDTL-BIRS model. The results imply that CKHDTL-BIRS model yielded improved outcomes over MN-SSAE model.
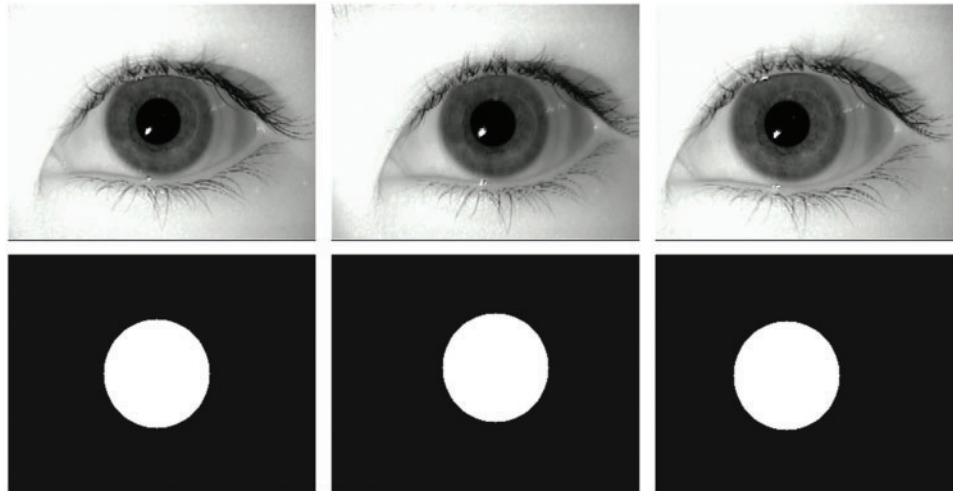
**Figure 3:** Sample images

**Table 1:** Results of the analysis of MN-SSAE model and CKHDTL-BIRS technique under different measures and runs

| No. of runs | Accuracy | Precision | Recall | F1-Score | AUC |
|---|---|---|---|---|---|
| MN-SSAE | | | | | |
| Run-1 | 99.15 | 99.01 | 98.89 | 99.31 | 98.93 |
| Run-2 | 98.85 | 98.85 | 99.29 | 99.38 | 99.17 |
| Run-3 | 99.17 | 99.17 | 99.07 | 99.26 | 99.33 |
| Run-4 | 99.21 | 99.17 | 99.31 | 99.29 | 99.28 |
| Run-5 | 99.00 | 99.32 | 98.97 | 99.28 | 98.84 |
| CKHDTL-BIRS | | | | | |
| Run-1 | 98.00 | 99.09 | 98.93 | 99.01 | 99.39 |
| Run-2 | 99.03 | 99.32 | 99.12 | 98.89 | 99.29 |
| Run-3 | 99.43 | 99.60 | 99.52 | 99.33 | 99.52 |
| Run-4 | 98.93 | 99.22 | 99.12 | 99.22 | 99.06 |
| Run-5 | 99.22 | 99.18 | 99.29 | 99.10 | 98.98 |

Fig. 4 highlights the IR outcomes of MN-SSAE model in terms of $accu_y$, $prec_n$, and $reca_l$. The results infer that MN-SSAE model offered effective results under all runs. For instance, on run-1, MN-SSAE model achieved $accu_y$, $prec_n$, and $reca_l$ values such as 99.15%, 99.01%, and 98.89% respectively. Simultaneously, on run-3, MN-SSAE approach accomplished $accu_y$, $prec_n$, and $reca_l$ values such as 99.17%, 99.17%, and 99.07% respectively. Followed by, on run-5, MN-SSAE model attained $accu_y$, $prec_n$, and $reca_l$ values such as 99%, 99.32%, and 98.97% correspondingly.
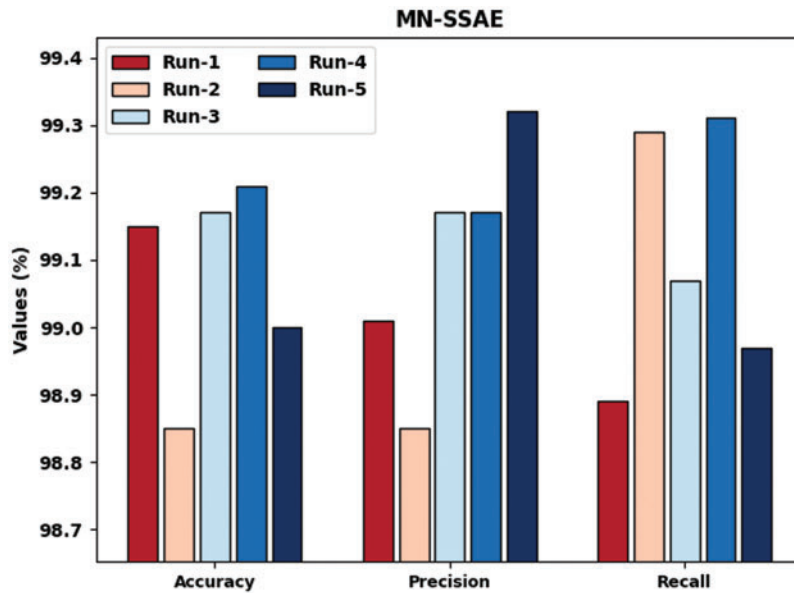
**Figure 4:** Results of the analysis of MN-SSAE technique under distinct runs

Fig. 5 highlights the IR outcomes of MN-SSAE technique with respect to $F1_{score}$ and $AUC$. The results infer that MN-SSAE model offered effectual results under all runs. For instance, on run-1, MN-SSAE method offered $F1_{score}$ and $AUC$ values such as 99.31% and 98.93% correspondingly. Eventually, on run-3, MN-SSAE approach yielded $F1_{score}$ and $AUC$ values such as 99.26% and 99.33% respectively. At last, on run-5, MN-SSAE model provided $F1_{score}$ and $AUC$ values such as 99.28% and 98.84% correspondingly.
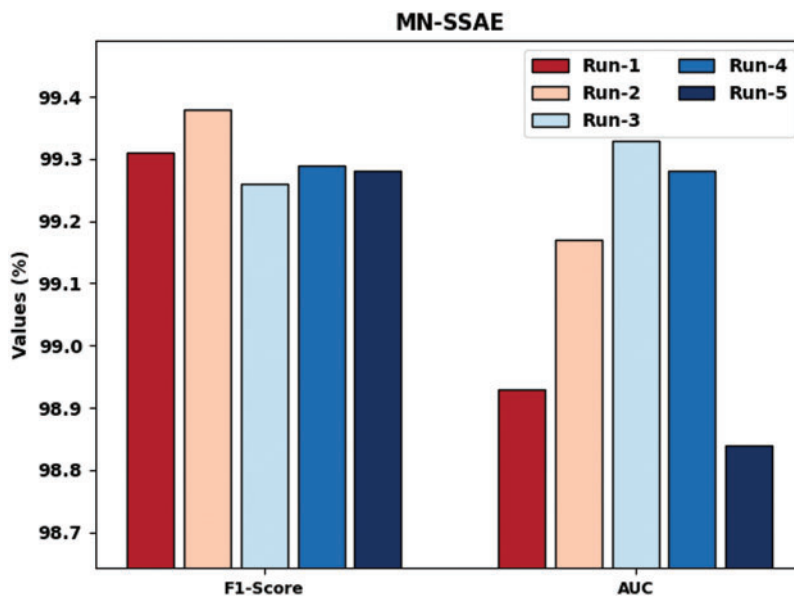


**Figure 5:** $F1_{score}$ and AUC analyses results of MN-SSAE technique under distinct runs

Fig. 6 examines the IR outcomes of CKHDTL-BIRS approach with respect to $accu_y$, $prec_n$, and $reca_l$. The results reveal that the proposed CKHDTL-BIRS method yielded effectual results under all runs. For instance, on run-1, CKHDTL-BIRS system attained $accu_y$, $prec_n$, and $reca_l$ such as 98%, 99.09%, and 98.93% respectively. In addition, on run-3, the proposed CKHDTL-BIRS model accomplished $accu_y$, $prec_n$, and $reca_l$ values such as 99.43%, 99.32%, and 99.14% respectively. Followed by, on run-5, CKHDTL-BIRS technique attained $accu_y$, $prec_n$, and $reca_l$ values such as 99.22%, 99.18%, and 99.29% correspondingly.
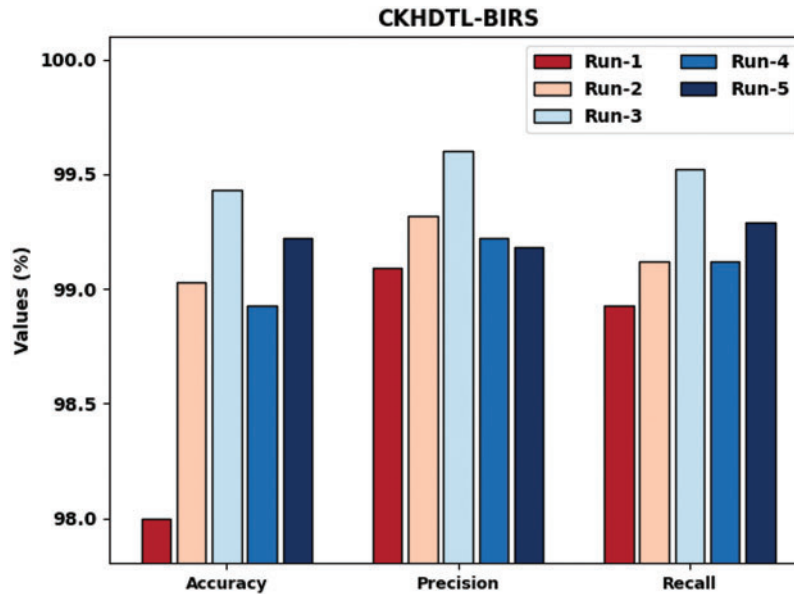


**Figure 6:** Results of the analysis of CKHDTL-BIRS technique under distinct runs

Fig. 7 demonstrates the IR outcomes achieved by CKHDTL-BIRS system in terms of $F1_{score}$ and Area Under the Curve (AUC). The outcomes infer that the proposed CKHDTL-BIRS model achieved effective results under all runs. For instance, on run-1, CKHDTL-BIRS technique yielded $F1_{score}$ and $AUC$ values such as 99.01% and 99.39% correspondingly. Moreover, on run-3, CKHDTL-BIRS model accomplished $F1_{score}$ and $AUC$ values such as 99.33% and 99.52% respectively. Eventually, on run-5, CKHDTL-BIRS method offered $F1_{score}$ and $AUC$ values such as 99.10% and 98.98% correspondingly.

A brief comparative study was conducted between CKHDTL-BIRS model and the existing models while the results are shown in Tab. 2. Fig. 8 reports the detailed comparative $accu_y$ and AUC inspection results accomplished by CKHDTL-BIRS and other recent models. The results imply that J48 and Spider Monkey Optimization (SMO) models achieved the least values of $accu_y$ and AUC. Followed by, Linear Support Vector Classifier (SVC) model gained a slightly enhanced $accu_y$ and AUC. Along with that, Random Forest (RF) and Cat Boost models reached closer $accu_y$ and AUC values. Though MN-SSAE model produced an $accu_y$ of 99.21% and an AUC of 99.17%, the proposed CKHDTL-BIRS model gained the maximum performance with an $accu_y$ of 99.43% and an AUC of 99.60% respectively.
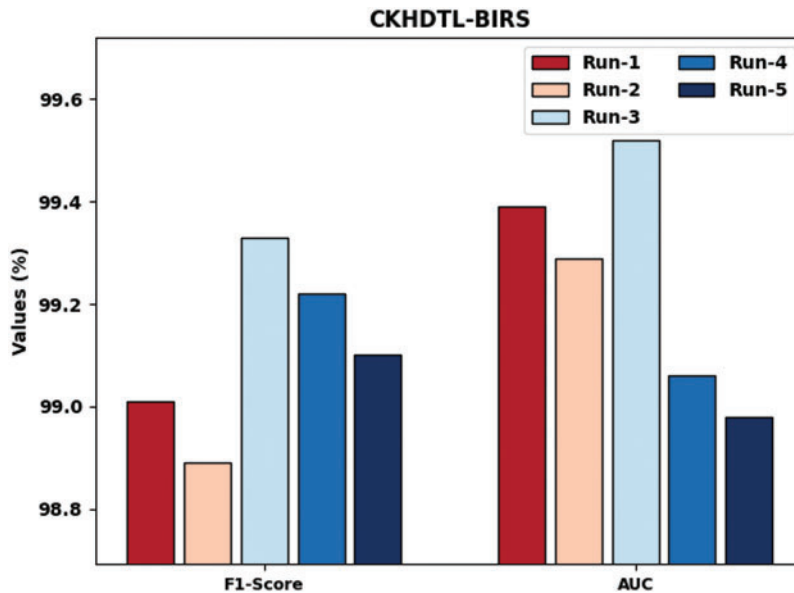
**Figure 7:** $F1_{score}$ and AUC analyses results of CKHDTL-BIRS technique under distinct runs

**Table 2:** Comparative analysis results achieved by CKHDTL-BIRS and other existing methods

| Methods | Accuracy | Precision | Recall | F1-Score | AUC |
|---|---|---|---|---|---|
| J48 Algorithm | 98.23 | 98.12 | 95.19 | 96.94 | 96.84 |
| SMO Algorithm | 98.35 | 98.02 | 94.76 | 97.16 | 96.86 |
| SVC Algorithm | 98.59 | 96.00 | 99.00 | 96.48 | 97.50 |
| Rand. forest | 98.85 | 98.45 | 97.78 | 97.95 | 98.80 |
| Cat-boost | 98.72 | 98.65 | 99.19 | 99.08 | 97.42 |
| MN-SSAE | 99.21 | 99.17 | 99.31 | 99.29 | 99.28 |
| CKHDTL-BIRS | 99.43 | 99.60 | 99.52 | 99.33 | 99.52 |

Fig. 9 portrays the detailed comparative $prec_n$, $reca_l$, and $F1_{score}$ analyses results accomplished by CKHDTL-BIRS model and other recent models. The outcomes expose that J48 and SMO models exhibited lesser $prec_n$, $reca_l$, and $F1_{score}$ values. Likewise, SVC model gained somewhat enhanced $prec_n$, $reca_l$, and $F1_{score}$ values. Also, RF and Cat Boost techniques attained closer values of $prec_n$, $reca_l$, and $F1_{score}$. Though MN-SSAE methodology produced $prec_n$, $reca_l$, and $F1_{score}$ values such as 99.17%, 99.31%, and 99.29%, the proposed CKHDTL-BIRS system accomplished the maximum performance with $prec_n$, $reca_l$, and $F1_{score}$ values such as 99.60%, 99.52%, and 99.33% correspondingly. Based on the interpreted outcomes and further discussions, it is confirmed that the proposed CKHDTL-BIRS model achieved maximum performance over other approaches.
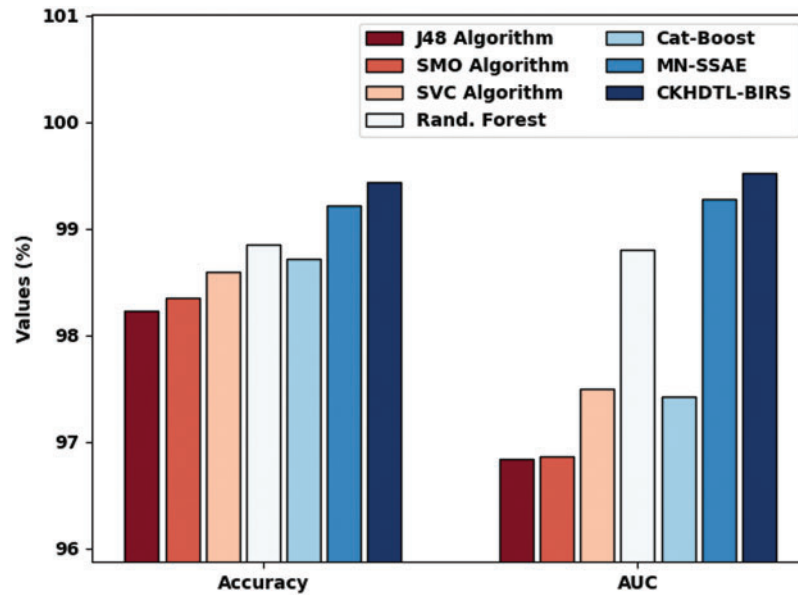
**Figure 8:** $Acc_y$ and AUC analyses results of CKHDTL-BIRS and other existing methodologies
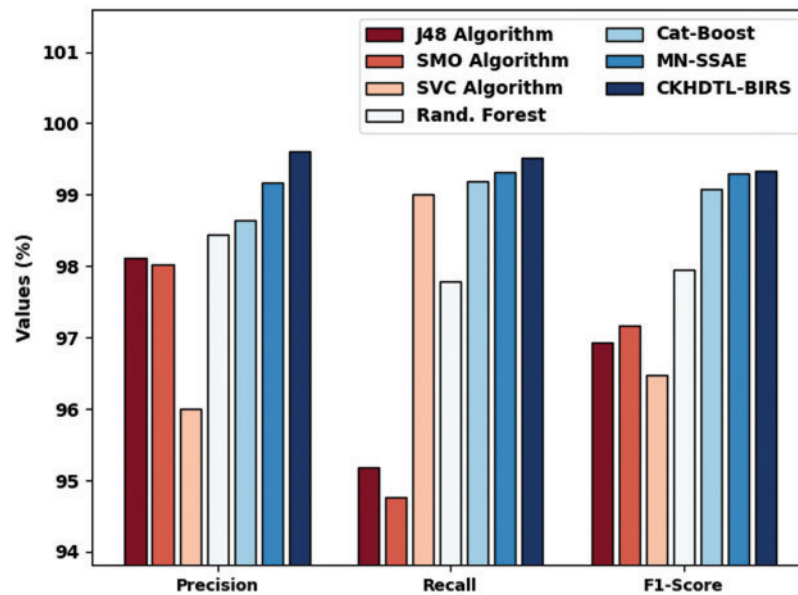


**Figure 9:** Comparative analysis results of CKHDTL-BIRS and other existing approaches

## 4  Conclusion

In this study, a novel CKHDTL-BIRS technique has been developed to recognize and classify iris images for biometric verification. The proposed CKHDTL-BIRS model initially performs MF to preprocess the images after which segmentation process is employed to localize iris regions. Besides, MobileNet model is also utilized to generate a set of useful feature vectors. Moreover, SSAE model is applied for classification. At last, CKH algorithm is exploited for optimization of the parameters

involved in SSAE approach. The proposed CKHDTL-BIRS model was experimentally validated using benchmark dataset and the outcomes were examined under several aspects. The comparison study outcomes established the enhanced performance of CKHDTL-BIRS model than the existing algorithms since the proposed model achieved the maximum $prec_n$, $reca_l$, and $F1_{score}$ values such as 99.60%, 99.52%, and 99.33% correspondingly. In future, deep instance segmentation approaches can be employed to improve the recognition performance of the presented model.

**Conflicts of Interest:** The authors declare that they have no conflicts of interest to report regarding the present study.

## References

[1]    A. S. A. Waisy, R. Qahwaji, S. Ipson, S. Al-Fahdawi and T. A. Nagem, "A Multi-biometric iris recognition system based on a deep learning approach," *Pattern Analysis and Applications*, vol. 21, no. 3, pp. 783–802, 2018.

[2]    A. Boyd, S. Yadav, T. Swearingen, A. Kuehlkamp, M. Trokielewicz *et al.,* "Post-mortem iris recognition—a survey and assessment of the state of the art," *IEEE Access*, vol. 8, pp. 136570–136593, 2020.

[3]    M. W. Sun, G. C. Zhang, X. R. Zhang, X. Zhang and N. N. Ge, "Fine-grained vehicle type classification using lightweight convolutional neural network with feature optimization and joint learning strategy," *Multimedia Tools and Applications*, vol. 80, no. 20, pp. 30803–30816, 2021.

[4]    W. Sun, X. Chen, X. R. Zhang, G. Z. Dai, P. S. Chang *et al.,* "A Multi-feature learning model with enhanced local attention for vehicle re-identification," *Computers, Materials & Continua*, vol. 69, no. 3, pp. 3549–3560, 2021.

[5]    V. C. Kagawade and S. A. Angadi, "A new scheme of polar fast Fourier transform code for iris recognition through symbolic modelling approach," *Expert Systems with Applications*, vol. 197, pp. 116745, 2022.

[6]    J. R. Malgheet, N. B. Manshor, L. S. Affendey and A. B. A. Halin, "Iris recognition development techniques: A comprehensive review," *Complexity*, vol. 2021, pp. 1–32, 2021.

[7]    M. B. Lee, J. K. Kang, H. S. Yoon and K. R. Park, "Enhanced iris recognition method by generative adversarial network-based image reconstruction," *IEEE Access*, vol. 9, pp. 10120–10135, 2021.

[8]    Y. Chen, Z. Zeng, H. Gan, Y. Zeng and W. Wu, "Non-segmentation frameworks for accurate and robust iris recognition," *Journal of Electronic Imaging*, vol. 30, no. 3, pp. 033002, 2021.

[9]    B. Muthazhagan and S. Sundaramoorthy, "Ameliorated face and iris recognition using deep convolutional networks," in *Machine Intelligence and Big Data Analytics for Cybersecurity Applications, Studies in Computational Intelligence Book Series*, Springer, Cham, vol. 919, pp. 277–296, 2021.

[10]  S. Lei, B. Dong, A. Shan, Y. Li, W. Zhang *et al.,* "Attention meta-transfer learning approach for few-shot iris recognition," *Computers & Electrical Engineering*, vol. 99, pp. 107848, 2022.

[11]  T. Zhao, Y. Liu, G. Huo and X. Zhu, "A deep learning iris recognition method based on capsule network architecture," *IEEE Access*, vol. 7, pp. 49691–49701, 2019.

[12]  S. Adamović, V. Miškovic, N. Maček, M. Milosavljević, M. Šarac *et al.,* "An efficient novel approach for iris recognition based on stylometric features and machine learning techniques," *Future Generation Computer Systems*, vol. 107, pp. 144–157, 2020.

[13]  N. Ahmadi, M. Nilashi, S. Samad, T. A. Rashid and H. Ahmadi, "An intelligent method for iris recognition using supervised machine learning techniques," *Optics & Laser Technology*, vol. 120, pp. 105701, 2019.

[14]  K. Wang and A. Kumar, "Toward more accurate iris recognition using dilated residual features," *IEEE Transactions on Information Forensics and Security*, vol. 14, no. 12, pp. 3233–3245, 2019.

[15]  E. G. Llano and A. M. Gonzalez, "Framework for biometric iris recognition in video, by deep learning and quality assessment of the iris-pupil region," *Journal of Ambient Intelligence and Humanized Computing*, pp. 1–13, 2021, Article in press, https://doi.org/10.1007/s12652-021-03525-x.

[16] Y. Li, H. Huang, Q. Xie, L. Yao and Q. Chen, "Research on a surface defect detection algorithm based on MobileNet-SSD," *Applied Sciences*, vol. 8, no. 9, pp. 1678, 2018.

[17] Y. Qi, C. Shen, D. Wang, J. Shi, X. Jiang *et al.,* "Stacked sparse autoencoder-based deep network for fault diagnosis of rotating machinery," *IEEE Access*, vol. 5, pp. 15066–15079, 2017.

[18] B. A. Y. Alqaralleh, T. Vaiyapuri, V. S. Parvathy, D. Gupta, A. Khanna *et al.,* "Blockchain-assisted secure image transmission and diagnosis model on internet of medical things environment," *Personal and Ubiquitous Computing*, 2021, Article in press, https://doi.org/10.1007/s00779-021-01543-2.

[19] B. A. Y. Alqaralleh, S. N. Mohanty, D. Gupta, A. Khanna, K. Shankar *et al.,* "Reliable multi-object tracking model using deep learning and energy efficient wireless multimedia sensor networks," *IEEE Access*, vol. 8, pp. 213426–213436, 2020.

[20] G. G. Wang, L. Guo, A. H. Gandomi, G. S. Hao and H. Wang, "Chaotic krill herd algorithm," *Information Sciences*, vol. 274, pp. 17–34, 2014.